:18

LA-UR- 97-5014

Title: THICK-TARGET NEUTRON, g-RAY, AND RADIONUCLIDE PRODUCTION FOR PROTONS BELOW 12 MEV ON NICKEL AND CARBON BEAM-STOPS

CONF-971125--

Author(s): M.B. Chadwick, T-2, MS-B283, Los Alamos National Laboratory, P.O. Box 1663, Los Alamos, NM 87545, USA
P. G. Young, T-2, MS-B283, Los Alamos National Laboratory, P.O. Box 1663, Los Alamos, NM 87545, USA
W. B. Wilson, T-2, MS-B283, Los Alamos National Laboratory, P.O. Box 1663, Los Alamos, NM 87545, USA

Submitted to: Proceedings of the American Nuclear Society Winter Meeting, Albuquerque, New Mexico, November 19, 1997.

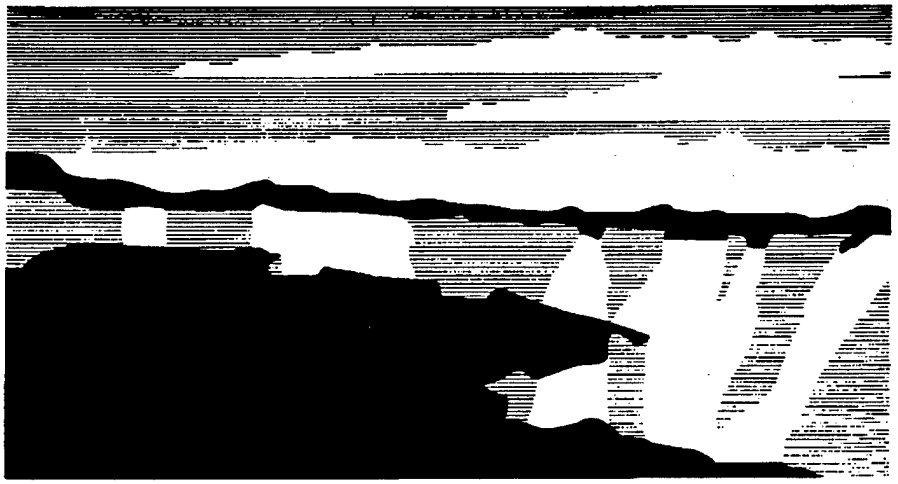

Los Alamos
NATIONAL LABORATORY

Form No. 836 R5
ST 2629 10/91

DISCLAIMER

THICK-TARGET NEUTRON, γ-RAY, AND RADIONUCLIDE PRODUCTION FOR PROTONS BELOW 12 MEV ON NICKEL AND CARBON BEAM-STOPS

M. B. Chadwick, P.G. Young, and W.B. Wilson
University of California
Theoretical Division
Los Alamos National Laboratory
Los Alamos, NM 87545
Tel. No. (505)667-9877

Abstract

Nuclear model calculations using the GNASH code are described for protons below 12 MeV incident on nickel and carbon isotopes, for beam-stop design in the Los Alamos Accelerator Production of Tritium Low Energy Demonstration Accelerator (LEDA) project. The GNASH calculations apply Hauser-Feshbach and preequilibrium reaction theories and can make use of pre-calculated direct reaction cross sections to low-lying residual nucleus states. From calculated thin-target cross sections, thick target 6.7 MeV and 12 MeV proton-induced production of neutrons, gamma-rays, and radionuclides are determined. Emission spectra of the secondary neutrons and gamma-rays are also determined. The model calculations are validated through comparisons with experimental thin– and thick–target measurements. The results of this work are being utilized as source terms in MCNP analyses for LEDA.

1 Introduction

Nickel and carbon are currently being considered for use as beam stop materials for the Los Alamos Low Energy Demonstration Accelerator (LEDA), for the Accelerator Production of Tritium (APT) project. LEDA will demonstrate the feasibility of producing a high-current proton beam for APT. The energy to which protons will be accelerated in LEDA is relatively low: an initial energy of 6.7 MeV is planned, with a possible increase to 12 MeV. Nickel and carbon are attractive beam-stop materials since proton-induced neutron production, which should be minimized as far as possible because of radiation protection considerations, is below threshold at 6.7 MeV for the major nickel isotopes (^{58,60}Ni), and below threshold at 6.7 and 12 MeV for the major carbon isotope (^{12}C).

This report summarizes nuclear model calculations for protons incident on ^{58,60,61,62,64}Ni and ^{12,13}C isotopes, for incident energies up to 12 MeV. Calculations are performed using the GNASH code [1], which applies Hauser-Feshbach equilibrium and exciton preequilibrium theories. These calculations are benchmarked against measured data, to validate the accuracy of the theoretical predictions. After the calculation of these "thin target" cross sections, thick-target neutron, gamma-ray, and radionuclide yields are determined for 6.7 MeV and 12.0 MeV incident energies.

2 Proton reactions on Nickel

2.1 Experimental data

Experimental data for proton-induced cross sections on Ni isotopes below 12 MeV were obtained from the CSISRS database from the National Nuclear Data Center at Brookhaven National Laboratory [2].

The most important measurements for benchmarking our model calculations are those of Kaufman (1960), Levkovskij (1991), Tanaka (1959,1972), Birjukov (1980), Blosser (1955), Sudar (1993), Antropov (1992), Johnson (1960), Szelecsenyi (1993), Sevior (1983), and Qaim (1995) [2]:

- Data for the p+Ni nonelastic cross section (above 8 MeV).
- (p,n) excitation function data for ^{60,61,62,64}Ni (but no such data exists for ^{58}Ni).
- (p,α) excitation function data for ^{58,60,61,64}Ni (but no such data exists for ^{62}Ni).
- An inclusive neutron emission spectrum for ^{58}Ni(p,xn) at 22 MeV - a higher energy than of direct relevance here, but useful for testing

the model calculations, especially since (p,n) excitation function data do not exist for ^{58}Ni.

2.2 Summary of Model Calculations

The GNASH code has been described in Ref. [1]. At the energies studied here ($\leq$ 12 MeV) equilibrium emission is the dominant reaction mechanism, with relatively small contributions from preequilibrium emission. An optical model is used to determine transmission coefficients for use in the Hauser-Feshbach GNASH calculations, as well as the reaction cross section. For neutrons and protons, the optical potential of Harper *et al.* [3] is used, which is a potential developed for Ni. For deuterons, the global potential of Perey was used [4], and for alpha particles the potential of Strohmaier and Uhl was used [5]. Gamma-ray transmission coefficients were obtained from the formalism of Kopecky and Uhl [6]. Continuum nuclear level densities were taken from the Gilbert-Cameron formalism [7], using the Cook systematics [8], matched continuously onto low-lying discrete levels taken from the ENSDF compilations [2]. In most cases the default level density parameters were found to provide satisfactory cross section predictions. However, the default level density and pairing parameters were modified to improve agreement with data for the following nuclides: ^{58}Ni, a=6.0; ^{61}Cu, a=7.5, Δ=1.0. The preequilibrium matrix element for damping transitions was taken as 175 MeV^3, chosen to optimize the preequilibrium spectra measured for higher-incident reactions (e.g. the 65 MeV Ni(p,xp) data of Sakai [2]).

2.3 Calculations compared to data

The experimental data summarized in Sec. 2.1 are important for guiding the model calculations (for instance, as mentioned above, in two cases the level densities were adjusted to improve agreement with data), and to validate the GNASH code's predictions.

At the lower incident proton energies, in many cases there are just three reactions that are dominant: (p,p'), (p,α), and (p,n). No measurements exist for the (p,p') channel below 12 MeV, since the residual nucleus is the same as the (stable) target nucleus and activation methods cannot be used. However, since our calculations predict the total nonelastic cross section rather well (See Fig. 1), if our calculations account for measured (p,n) and (p,α) data, then one can be confident that the (p,p') channel is also determined accurately.

Below we summarize features seen in the comparisons with measurements shown in Figs. 2-6:

p+^{58}Ni In Fig. 2, the alpha emission channel is seen to describe the data well. No data exists for the (p,n) excitation function, but Fig. 2 shows that the neutron emission spectrum at 22 MeV is described fairly well. The preequilibrium spectrum is somewhat overpredicted, but this has only a minor impact below 12 MeV.

p+^{60}Ni In Fig. 3, the alpha and neutron emission channels are seen to describe the measurements fairly well. The structure seen in the (p,n) excitation function between 8 and 10 MeV is due to the effects of level densities and transmission coefficients in the competition between neutron and proton emission. The data do not show such a marked structure, though the fluctuations in the measured values are too great to be sure that no structure exists.

p+^{61}Ni In Fig. 4, both the (p,n) and (p,α) channels are described fairly well, though the agreement was obtained by increasing the ^{61}Cu level density from its default value (see above). We could have further increased the ^{61}Cu level density to increase neutron emission (and lower alpha emission) above 9 MeV. However, neutron emission in elemental nickel is important from this isotope below 6.7 MeV (since neutron production from the major isotopes is below threshold here), but above this energy it is relatively unimportant due the opening-up of neutron channels in the abundant ^{58,60}Ni isotopes.

p+^{62}Ni In Fig. 5, the (p,n) excitation function is seen to agree reasonably well with the data. There is a hint of an overprediction of this excitation function below 7 MeV. But we were unable to decrease our results since at these low energies the reactions are taking place predominantly in the discrete-level region, so that level density parameters have no influence.

p+^{64}Ni In Fig. 6, our calculations of the (p,n) and (p,α) channels are seen to describe the measurements well.

Calculated neutron production from the five isotopes is shown on the left side of Fig. 7. The neutron production cross sections are multiplied by

the fractional isotopic abundances and shown on the right side of Fig. 7, to indicate the important sources of neutron production in elemental nickel. From this it is clear that below 6.7 MeV, neutron production only occurs from the minor isotopes (^{61,62,64}Ni). Between 6.7 and 12 MeV, neutron production from ^{60}Ni becomes dominant, with ^{62,58}Ni also being significant.

Estimates of the accuracy of our calculated neutron production can be obtained by noting that from the r.h.s. of Fig. 7, neutron production in elemental nickel is most important from ^{62}Ni below about 7 MeV and from ^{60}Ni between 7 and 12 MeV, and that comparisons with measurements for these reactions in Figs. 3, 5 indicate accuracies of better than 25%. Thus we expect our calculations of neutron production (both think and thick target) to be accurate to better than 25%.

2.4 Thick-target calculations

From our calculated (thin-target) proton-induced cross sections, we determined thick-target yields of neutrons, gamma-rays, and radionuclides. To do this, GNASH calculations were performed for all incident energies below 12 MeV on a 0.1-MeV grid, and the results appropriately averaged according to the slowing down calculated using the stopping powers of Anderson and Ziegler [9].

Results for total neutron, gamma-ray, and radionuclide production are given in Table I. Our results for radionuclide production agree well with those in the compilation of Young and Rose [10], which provides results below 10 MeV for the production of Co and Cu isotopes, with the exception of the ^{60}Ni(p,n)^{60}Cu cross section where the Young and Rose results are approximately five times larger. In discussions with Dr. F.C. Young we have learned of an error (overprediction) in their work for this reaction. Our results for neutron production from elemental nickel at 12 MeV is somewhat higher than the measurement of Daruga and Matusevich [11] at 11.5 MeV of 74e-6 neutrons/proton (experiment is approx 50% smaller, with an 18% uncertainty).However, since ^{60}Ni(p,xn) is the major contributor to the elemental nickel result at this energy (Fig. 7), and our thin-target calculations describe the data well (Fig. 3), we are confident in the validity of our thick-target calculations. Furthermore, Borchers *et al.* have measured thick target zero-degree neutron spectra on ^{58}Ni at 12 MeV, and our results are in good agreement. They find, for neutrons above their detector threshold of 0.7 MeV, a total forward-angle neutron production of approx. 1.6e-6 neutrons/proton.sr (1.e7 neutrons/sr-μC), compared to our calculated value of 1.3e-6 neutrons/proton.sr.

Angle-integrated thick target neutron spectra are shown in Fig. 8 for elemental nickel at 6.7 and 12 MeV, and for ^{58}Ni at 12 MeV. These neutron spectra are isotropic to a good approximation at these energies.

3 Proton reactions on Carbon

Since the ^{12}C(p,n) threshold is at 19.6 MeV, thick-target neutron production for protons is due entirely to reactions on ^{13}C. However, our calculations include both ^{12}C and ^{13}C since ^{12}C is an important source of gamma-rays and radionuclides.

Details of the optical model and level density parameters for our GNASH calculations on carbon are described in Ref. [12]. In addition to Hauser-Feshbach and preequilibrium reaction mechanisms, ^{13}C(p,n) direct reaction cross sections to low-lying states in ^{13}N were evaluated from measurements and included incorporated into the GNASH calculations [13, 14, 15, 16]. This proved to be important for correctly determining the magnitude of neutron production.

Thick-target neutron, gamma-ray, and radionuclide production for 12 MeV protons was obtained from our GNASH calculations, and appropriately weighted according to isotopic composition for elemental carbon. Results for the production cross sections are presented in Table II. The calculated results for the total neutron production as a function of incident energy are shown in Fig. 9. Agreement with the measurements of Bair *et al.* (1981) [14] and Daruga and Matusevich (1970) [11] is seen to be good near 12 MeV. Differential neutron spectra measurements at 12 MeV by Borchers (1964) [17], at 0 and 90 degrees, are also shown in Fig. 9, and the agreement with our calculations is seen to be good. Our results for the thick-target ^{13}C$(p,n)^{13}$N reaction agree well with those shown in Young and Rose's compilation below 10 MeV [10].

Note that Fig. 9 indicates the neutron source to have a considerable anisotropy – this is largely due to the kinematical c.m. to lab transformation which has a significant effect for carbon (being light), resulting in an enhanced emission at forward angles. Integrating the neutron spectra over all emission energies gives an angular variation for

0^o : 90^o : 180^o of 1 : 0.42 : 0.23. For this reason, the angle-energy correlated distribution of the thick-target neutron source is provided for subsequent transport calculations, rather than assuming an isotropic source.

4 Conclusions

Nuclear model calculations using the GNASH code provide a reliable way to determine thich-target neutron, gamma-ray, and radionuclide production for beam-stop design in APT. In addition to predicting the production cross sections, the model calculations also predict emission spectra and angular distributions of the light secondary ejectiles, allowing them to be used as a source term for subsequent MCNP transport calculation [18]. We expect our predicted thick-target results to be accurate to better than 25%.

If one is restricted to using beam-stop material of elemental composition, neutron production in carbon is an order of magnitude smaller than nickel at 12 MeV, and a factor of 4 smaller at 6.7 MeV. Gamma-ray production is also smaller for carbon at 12 MeV, though it becomes larger than in nickel by about a factor of 2 at 6.7 MeV. If it were possible to obtain pure ^{58}Ni as a beam-stop material, at 6.7 MeV no neutron production occurs, and gamma-ray production is small. At 12 MeV, pure ^{58}Ni exhibits comparable levels of neutron and gamma-ray production to our predictions for elemental carbon.

Therefore, this study suggests that carbon may be the optimal choice for the LEDA beam stop, particularly if a beam energy of 12 MeV is anticipated, though for lower beam energies an isotopically-enriched ^{58}Ni beam-stop would be most attractive.

5 Acknowledgments

We gratefully acknowledge useful discussions with Drs. E. Pitcher and P. Ferguson.

References

[1] P.G. Young, E.D. Arthur, and M.B. Chadwick, Los Alamos National Laboratory document LA-MS-12343 (1992); M.B. Chadwick and P.G. Young, *Phys. Rev. C* **47**, 2255 (1993).

[2] Brookhaven National Laboratory National Nuclear Data Center.

[3] R.C. Harper and W.L. Alford, *J. Phys. G* **8**, 153 (1982).

[4] C.M. Perey and F.G. Perey, *Atomic Data and Nuclear data Tables* **17**, 1 (1976).

[5] B. Strohmaier and M. Uhl, *Proc. Int. Conf. on Nucl. Data for Science and Tech.*, Antwerp, 1982 (Reidel, Durdrecht, 1983) p. 552.

[6] J. Kopecky and M. Uhl, *Phys. Rev. C* **41**, 1941 (1990).

[7] A. Gilbert and A.G.W. Cameron, *Can J. Phys.* **43**, 1446 (1965).

[8] J.L. Cook, H. Ferguson, and A.R. Musgrove, *Aus. J. Phys.* **20**, 477 (1967).

[9] H.H. Anderson and J.F. Ziegler, Vol. 3 of *The Stopping and Ranges of Ions in Matter*, Pergamon Press, New York, NY (1978).

[10] F.C. Young and D.V. Rose, *Atomic Data and Nucl. Data Tables* **64** 223 (1996).

[11] V.K. Daruga and E.S. Matusevich, *Atomnaya Energiya* **29**. 456 (1970).

[12] M.B. Chadwick, M. Blann, L.J. Cox, P.G. Young, and A.S. Meigooni, *Nucl. Sci. Eng.* **123**, 17 (1996).

[13] P. Dagley, W. Haeberli, and J.X. Saladin, *Nucl. Phys.* **24**, 353 (1961).

[14] J.K. Bair, P.D. Miller, and B.W. Wieland, *Int. J. Appl. Rad. Iso.* **32**, 389 (1981).

[15] W.B. Wilson, Los Alamos National Laboratory Group T-2 memo T-2-M-1658 to T. Cole, LANSCE (LANL) (1985).

[16] P.G. Young, W.B. Wilson, and M.B. Chadwick, Los Alamos National Laboratory Group T-2 memo T-2-M-95-18 to G.J. Russel, LANSCE (LANL) (1995).

[17] R.R. Borchers, J.C. Overley, and R.M. Wood, *Nucl. In. Meth.* **30**, 73 (1964).

[18] J.F. Briesmeister, "MCNP – A general Monte Carlo N-Particle Transport Code", Los Alamos National Laboratory report LA-12625-M (1993).

Thick-target yields for p + Ni-58

Product	6.70 MeV	12.00 MeV
neutron	0.00E+00	1.78E-05
gammas	1.41E-04	2.94E-03
H - 1	1.04E-04	1.35E-03
H - 2	0.00E+00	5.96E-11
He- 4	9.14E-09	1.46E-05
Fe- 54	0.00E+00	1.16E-11
Co- 55	9.14E-09	1.46E-05
Co- 57	0.00E+00	1.98E-08
Ni- 57	0.00E+00	5.96E-11
Cu- 58	0.00E+00	1.78E-05

Thick-target yields for p + Ni-60

Product	6.70 MeV	12.00 MeV
neutron	0.00E+00	3.47E-04
gammas	1.85E-04	3.09E-03
H - 1	1.19E-04	1.03E-03
H - 2	0.00E+00	3.26E-09
He- 4	2.25E-07	3.98E-05
Fe- 56	0.00E+00	1.16E-11
Co- 57	2.25E-07	3.98E-05
Co- 59	0.00E+00	1.28E-13
Ni- 59	0.00E+00	3.26E-09
Cu- 60	0.00E+00	3.47E-04

Thick-target yields for p + Ni-61

Product	6.70 MeV	12.00 MeV
neutron	1.25E-04	9.52E-04
gammas	2.49E-04	3.29E-03
H - 1	7.41E-05	5.53E-04
H - 2	1.00E-15	1.61E-06
H - 3	0.00E+00	4.22E-16
He- 4	5.81E-07	7.06E-05
Fe- 57	0.00E+00	1.62E-12
Co- 57	0.00E+00	3.93E-10
Co- 58	5.81E-07	7.06E-05
Ni- 59	0.00E+00	4.22E-16
Ni- 60	1.00E-15	4.94E-05
Cu- 61	1.25E-04	9.04E-04

Thick-target yields for p + Ni-62

Product	6.70 MeV	12.00 MeV
neutron	1.34E-04	1.16E-03
gammas	2.36E-04	3.76E-03
H - 1	3.47E-05	3.09E-04
H - 2	0.00E+00	3.34E-08
H - 3	0.00E+00	7.97E-12
He- 4	2.29E-07	3.06E-05
Fe- 58	0.00E+00	1.40E-13
Co- 59	2.29E-07	3.06E-05
Ni- 60	0.00E+00	7.97E-12
Ni- 61	0.00E+00	3.49E-08
Cu- 62	1.34E-04	1.16E-03

Thick-target yields for p + Ni-64

Product	6.70 MeV	12.00 MeV
neutron	2.11E-04	1.53E-03
gammas	4.41E-04	4.76E-03
H - 1	1.92E-06	5.87E-05
H - 2	0.00E+00	1.49E-07
H - 3	0.00E+00	8.14E-09
He- 4	6.85E-08	1.16E-05
Co- 60	0.00E+00	7.04E-13
Co- 61	6.85E-08	1.16E-05
Ni- 62	0.00E+00	8.14E-09
Ni- 63	0.00E+00	1.78E-07
Cu- 63	0.00E+00	4.95E-05
Cu- 64	2.11E-04	1.43E-03

Thick-target yields for p + Ni-nat

Product	6.70 MeV	12.00 MeV
neutron	8.16E-06	1.69E-04
gammas	1.61E-04	3.03E-03
H - 1	1.04E-04	1.21E-03
H - 2	1.13E-17	2.16E-08
H - 3	0.00E+00	7.44E-11
He- 4	8.05E-08	2.23E-05
Fe- 54	0.00E+00	7.95E-12
Fe- 56	0.00E+00	3.02E-12
Fe- 57	0.00E+00	1.83E-14
Fe- 58	0.00E+00	5.03E-15
Co- 55	6.24E-09	9.94E-06
Co- 57	5.88E-08	1.04E-05
Co- 58	6.57E-09	7.98E-07
Co- 59	8.23E-09	1.10E-06
Co- 60	0.00E+00	6.41E-15
Co- 61	6.23E-10	1.06E-07
Ni- 57	0.00E+00	4.07E-11
Ni- 59	0.00E+00	8.51E-10
Ni- 63	0.00E+00	1.62E-09
Cu- 58	0.00E+00	1.21E-05
Cu- 60	0.00E+00	9.04E-05
Cu- 61	1.42E-06	1.02E-05
Cu- 62	4.82E-06	4.17E-05
Cu- 63	0.00E+00	4.50E-07
Cu- 64	1.92E-06	1.30E-05

Table I. Thick-target production (per-proton) of neutrons, gammas, and radionuclides for 6.7 and 12.0 MeV protons on pure nickel isotopes, and on elemental nickel.

Thick-target yields for p + C-12

Product	6.70 MeV	12.00 MeV
gammas	3.52E-04	1.89E-03
H - 1	3.52E-04	2.41E-03
He- 4	0.00E+00	1.38E-03
Be- 8	0.00E+00	6.64E-10

Thick-target yields for p + C-13

Product	6.70 MeV	12.00 MeV
neutron	1.91E-04	1.61E-03
gammas	7.47E-04	2.40E-03
H - 1	7.44E-04	2.74E-03
H - 2	1.70E-04	9.91E-04
He- 4	3.79E-06	2.26E-04
Li- 6	0.00E+00	3.01E-06
Be- 8	0.00E+00	1.31E-11
Be- 9	0.00E+00	2.99E-16
B - 10	3.79E-06	1.63E-04
C - 12	1.86E-04	2.10E-03
N - 13	1.75E-04	4.82E-04

Thick-target yields for p + C-nat

Product	6.70 MeV	12.00 MeV
neutron	2.10E-06	1.78E-05
gammas	3.56E-04	1.90E-03
H - 1	3.56E-04	2.41E-03
H - 2	1.87E-06	1.09E-05
He- 4	4.17E-08	1.37E-03
Li- 6	0.00E+00	3.31E-08
Be- 8	0.00E+00	6.56E-10
Be- 9	0.00E+00	3.29E-18
B - 10	4.17E-08	1.79E-06
N - 13	1.93E-06	5.30E-06

Table II. Thick-target production (per-proton) of neutrons, gammas, and radionuclides for 6.7 and 12.0 MeV protons on pure carbon isotopes, and on elemental carbon.

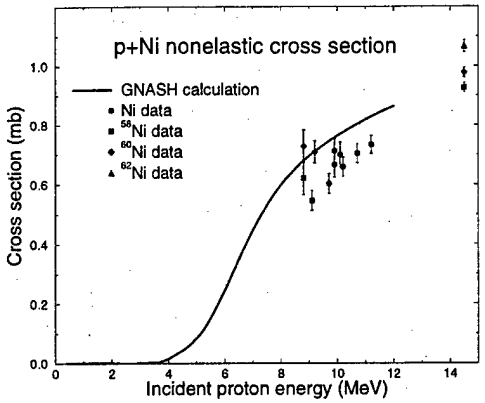

Figure 1: The calculated $p + Ni$ nonelastic cross section compared with measurements.

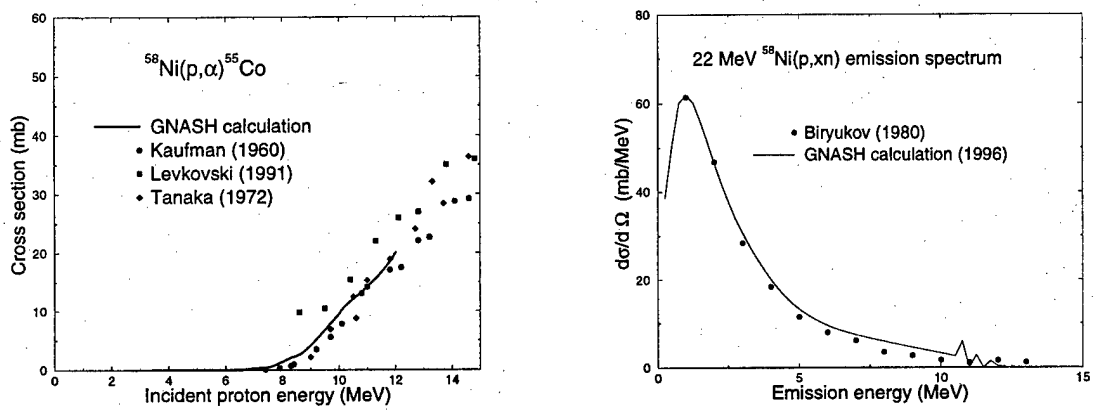

Figure 2: The excitation function for the reaction $^{58}\mathrm{Ni}(p,\alpha)$ reaction (l.h.s.), and the 22 MeV neutron emission spectrum in the $^{58}\mathrm{Ni}(p,xn)$ reaction (r.h.s.), compared with measurements.

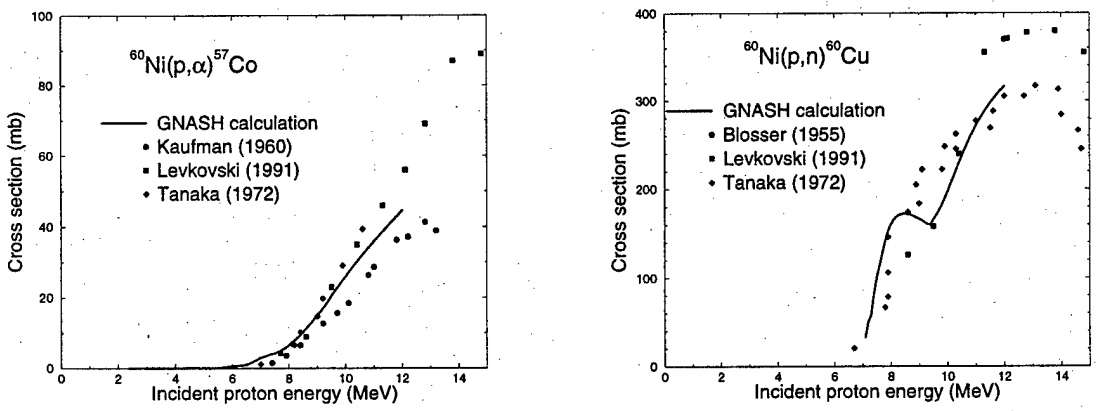

Figure 3: The excitation function for the reaction $^{60}\mathrm{Ni}(p,\alpha)$ reaction (l.h.s.), and the $^{60}\mathrm{Ni}(p,n)$ reaction (r.h.s.), compared with measurements.

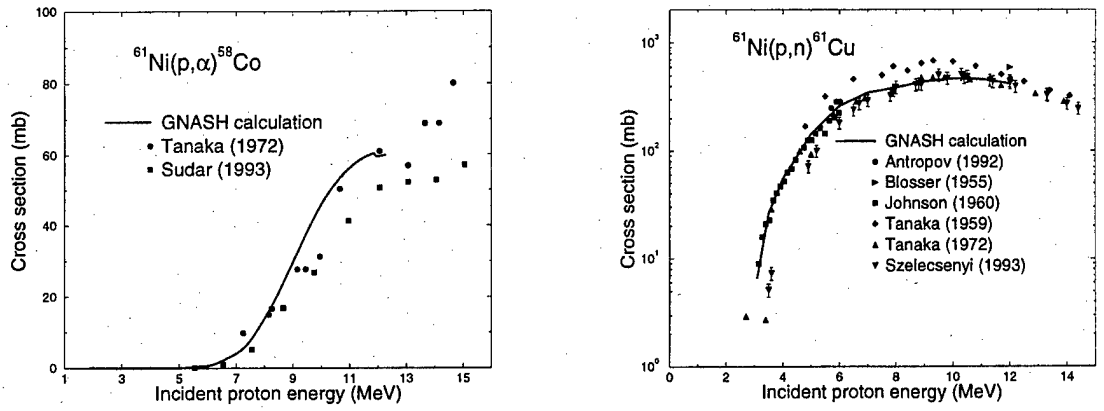

Figure 4: The excitation function for the reaction $^{61}\mathrm{Ni}(p,\alpha)$ reaction (l.h.s.), and the $^{61}\mathrm{Ni}(p,n)$ reaction (r.h.s.), compared with measurements.

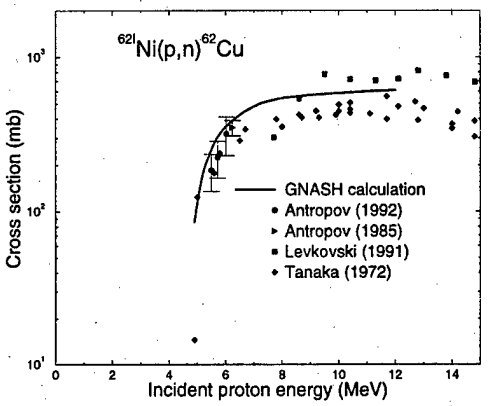

Figure 5: The excitation function for the reaction $^{62}\mathrm{Ni}(p,n)$ compared with measurements.

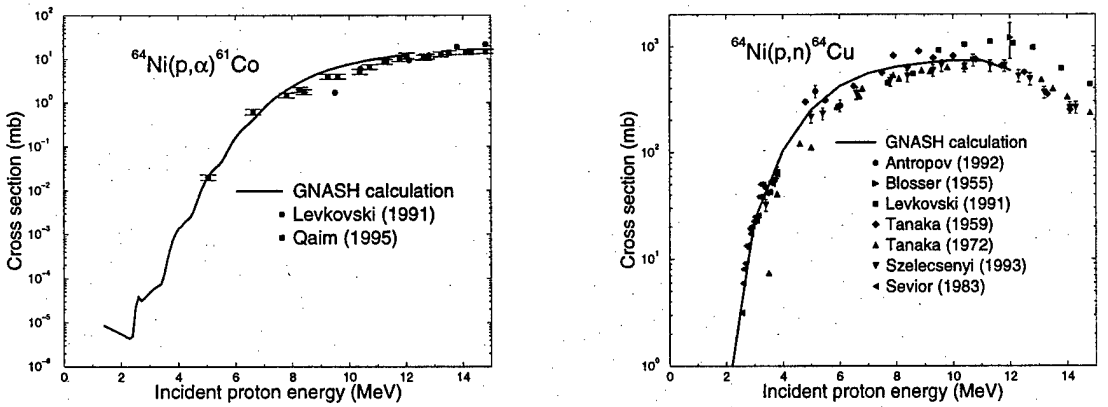

Figure 6: The excitation function for the reaction $^{64}\mathrm{Ni}(p,\alpha)$ reaction (l.h.s.), and the $^{64}\mathrm{Ni}(p,n)$ reaction (r.h.s.), compared with measurements.

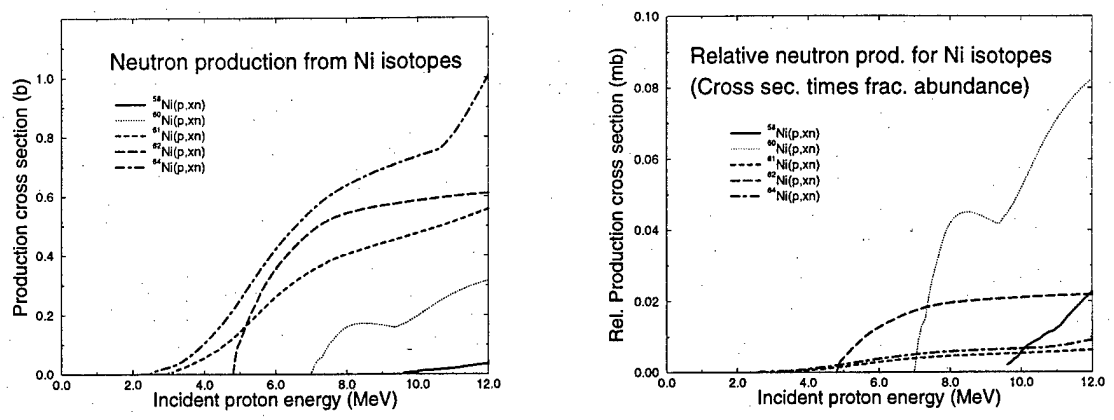

Figure 7: Neutron production as a function of incident proton energy for various Ni isotopes (l.h.s.), and these same values multiplied by the fractional natural isotopic abundances (r.h.s.).

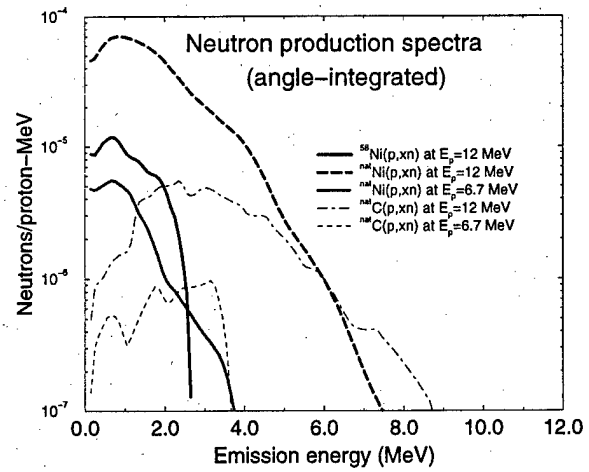

Figure 8: Calculated thick-target neutron spectra, for protons on nickel and carbon

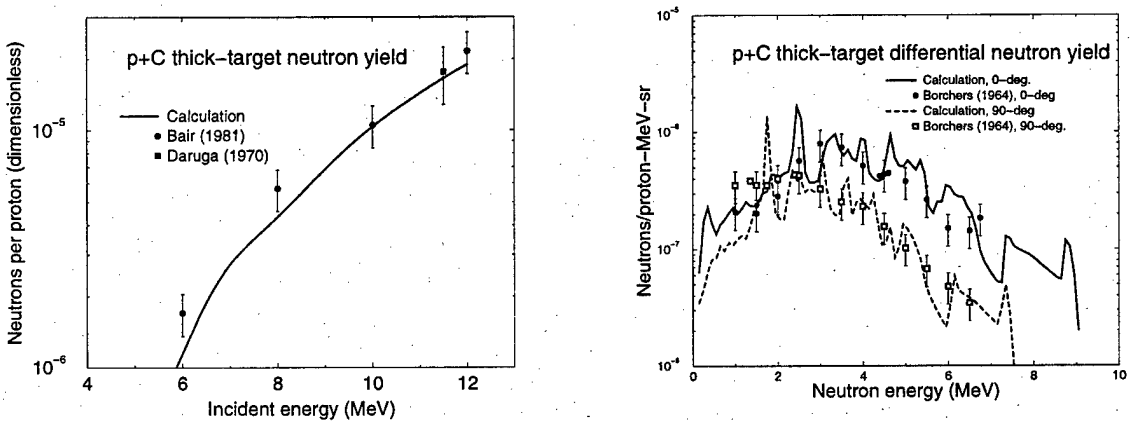

Figure 9: Calculated thick-target neutron production, and spectra, for protons on natural carbon, compared with measurements.

Report Number (14) LA-UR--97-5014
CONF-971125--

Publ. Date (11) 199803
Sponsor Code (18) DOE/ER, XF
UC Category (19) UC-413, DOE/ER

DOE